Electronic Supplementary Material (ESI) for Nanoscale.

Drying of electrically conductive hybrid polymer-gold nanorods studied with *in situ* microbeam GISAXS

Peng Zhang*[a], Beate Reiser[a], Lola González-García[a], Sebastian Beck[a], Juraj Drzic[a] and Tobias Kraus*[a,b]

[a] INM–Leibniz Institute for New Materials, Campus D2 2, 66123 Saarbrücken, Germany

[b] Colloid and Interface Chemistry, Saarland University, Campus D2 2, 66123 Saarbrücken, Germany

Corresponding authors: P. Zhang, zhangpeng3@mail.sysu.edu.cn; T. Kraus, tobias.kraus@leibniz-inm.de

Present address

P. Zhang: School of materials science and engineering, Sun Yat-sen University, 510275, Guangzhou, China

S1. Nanoparticle synthesis and solution preparation

Preparation of AuNR@CTAB solution

The synthesis of gold nanorods capped by cetylammoniumbromide (AuNR@CTAB) was adapted from a protocol by Ye et al.[1]. Briefly, 7.0 g of CTAB (⩾ 99%, Sigma-Aldrich, Germany), 1.234 g of sodium oleate (⩾ 99%, Sigma-Aldrich, Germany), 12.47 mg of silver nitrate (99.9%, ABCR, Germany), 100 mg tetrachloroauric acid trihydrate, 1.734 mL hydrochloric acid solution (32 wt.% in water, Sigma-Aldrich, Germany) and 14.1 mg of ascorbic acid (99%, Sigma-Aldrich, Germany) were sequentially dissolved in 500 mL water at 30 °C to yield a growth solution. Then 400 µL of a seed solution, prepared by reducing a 0.2 M CTAB, 0.5 mM tetrachloroauric acid solution with 1 mL of a 0.006 M sodium borohydride (⩾ 99%, Sigma-Aldrich, Germany) solution, were added to the growth solution. The resulting reaction mixture was left to react undisturbed for 16 h at 30 °C. The resulting dispersion was concentrated and purified by centrifugation and redispersion in 5 mM CTAB solution.

Preparation of AuNR@PEDOT:PSS solution

We employed a ligand exchange protocol previously developed in our group[2] that yields nanorods capped by poly(3,4-ethylenedioxythiophene) polystyrene sulfonate (PEDOT:PSS). Centrifugation of the AuNR@CTAB dispersion reduced the CTAB concentration to 250 µM at a gold concentration of 10 mg/mL. 5 mL of this AuNR@CTAB dispersion were immediately injected into 45 mL of a 0.9 mg/mL aqueous solution of PEDOT:PSS (formed by dissolving dry, re-dispersible pellets; resistance: 200-450 Ω/sq, Sigma-Aldrich, Germany) under vigorous stirring. After gentle stirring for 16 h at room temperature the excess of free ligands was removed and the AuNR@PEDOT:PSS solution was concentrated to a stock solution of 3.3 mg/mL (3.3 ± 0.1 mg/mL, measured with inductively coupled plasma optical emission spectrometry) by centrifugation.

Successful ligand exchange for CTAB by PEDOT:PSS in PEDOT:PSS@AuNR dispersion was confirmed by the following observations: a) the PEDOT:PSS@AuNR dispersion are colloidally stable at low temperature, while CTAB precipitates at lower temperatures; b) The resistivity of deposited lines of AuNR@PEDOT:PSS was 9.9×10^{-7} Ω m (39 Ω m /sq/mil), while lines prepared of rods carrying the original surfactant were insulating; c) the PEDOT:PSS@AuNRs dispersion had a negative zeta potential (-45 mV) while the CTAB@AuNRs dispersion has a positive zeta potential value of +25 mV. Additional details on the preparation and characterization of the polymer-AuNR hybrid nanoparticles, including spectroscopic analysis, can be found in previous work[2].

Preparing the AuNR@PEDOT:PSS solution for spray coating

The stock solution was diluted with water to 1 mg/mL AuNR@PEDOT:PSS dispersion that we used for the SAXS/GISAXS experiments.

S2. Structure of the as-prepared hybrid nanoparticles

a. Transmission Small-Angle X-ray Scattering (SAXS)

The transmission SAXS measurements were undertaken at the P03 beamline, with hybrid rod dispersion (1 mg/mL) held in the quartz capillary tubes (wall thickness 0.01 mm, Hilgenberg GmbH, Malsfeld, Germany). The exposure time was 10 s. The other measurement parameters were the same with those of GISAXS measurements mentioned in section S4.

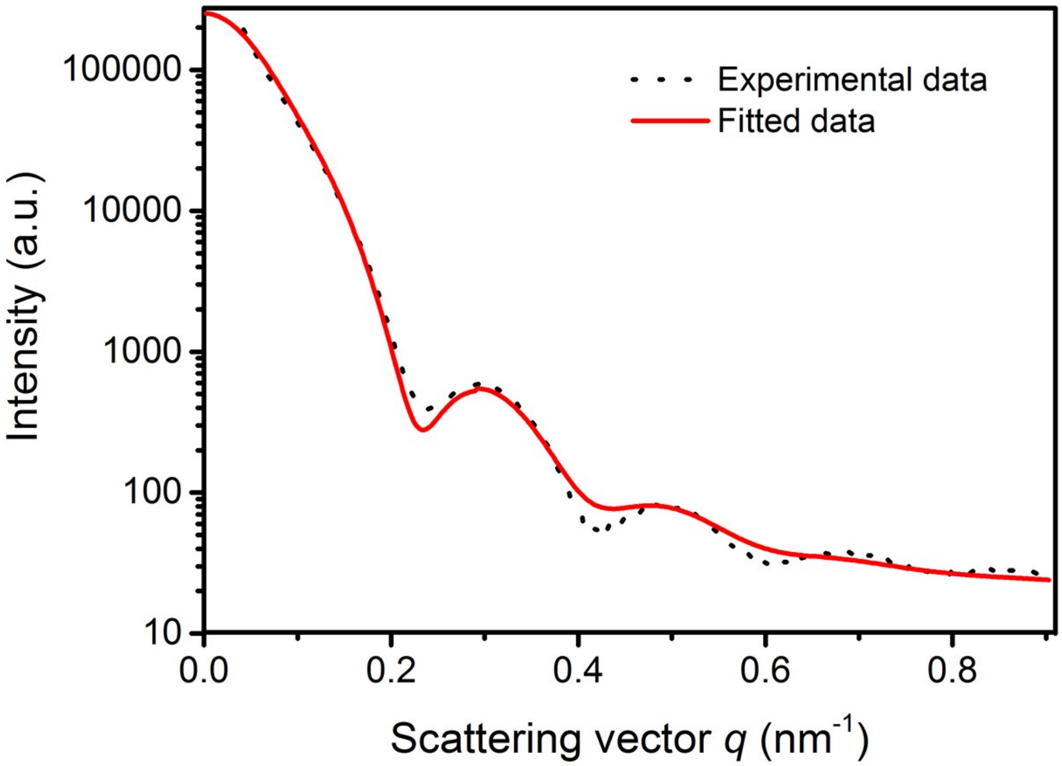

Figure S1. Transmission SAXS data (dotted line) and its fitting curve (solid line) of hybrid rod dispersed in water (1 mg/mL).

We analyzed the size of the AuNRs by fitting the SAXS data (Figure S1) using the Scatter[3] software. A cylindrical particle with a radius of 17.2 ± 2 nm and a length of 69.1 ± 10 nm fitted the experimental data well (Figure S1). It was not necessary to assume a lattice to obtain a good fit, indicating that there was no ordered packing of AuNR in the dispersions.

b. Transmission (TEM) and scanning electron micrographs (SEM) of particles

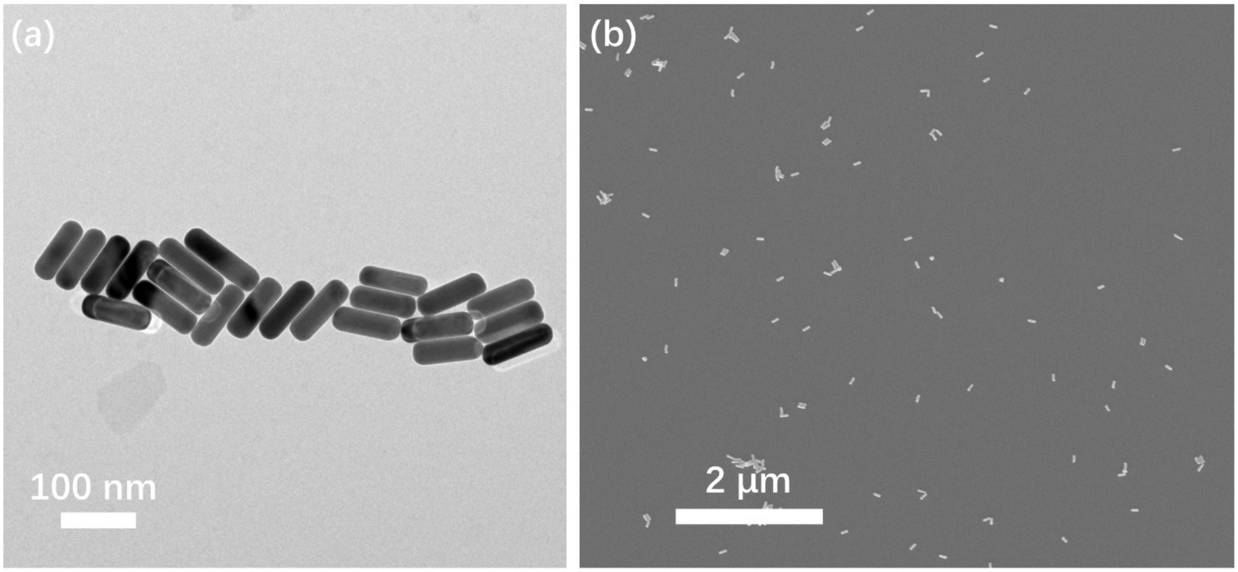

Figure S2. (a) Transmission electron micrograph and (b) scanning electron micrograph of dried hybrid nanoparticles immediately after synthesis.

The aqueous hybrid nanoparticle dispersion was diluted with water and drop-casted onto carbon-coated TEM grids or dip-coated on silicon substrates for SEM. The deposited films were dried in fume hood at room temperature for 24 h before they were imaged in the microscope.

S3. Air-brush spray deposition

The hybrid rod dispersion was atomized with compressed N_2 gas at pressure 1 bar. A commercial spray nozzle (Grafo T3, Harder & Steenbeck GmbH & Co. KG, Germany) was modified to adapt it to the beamline environment for *in situ* X-ray scattering measurements as shown in Figure S3. The spray time was set at 0.1 s, corresponding to a deposition of approximately 50 pL of dispersion. Previous work indicated that the central part of the spray cone had a diameter around 30 mm and caused a nearly homogeneous material deposition on the substrate.[4] The nozzle-to-substrate distance was 10 cm. Clean silicon wafers (<100> orientation, Si-mat Germnay) were used as substrates. The environmental temperature during the spray deposition was 25 ± 0.5 °C.

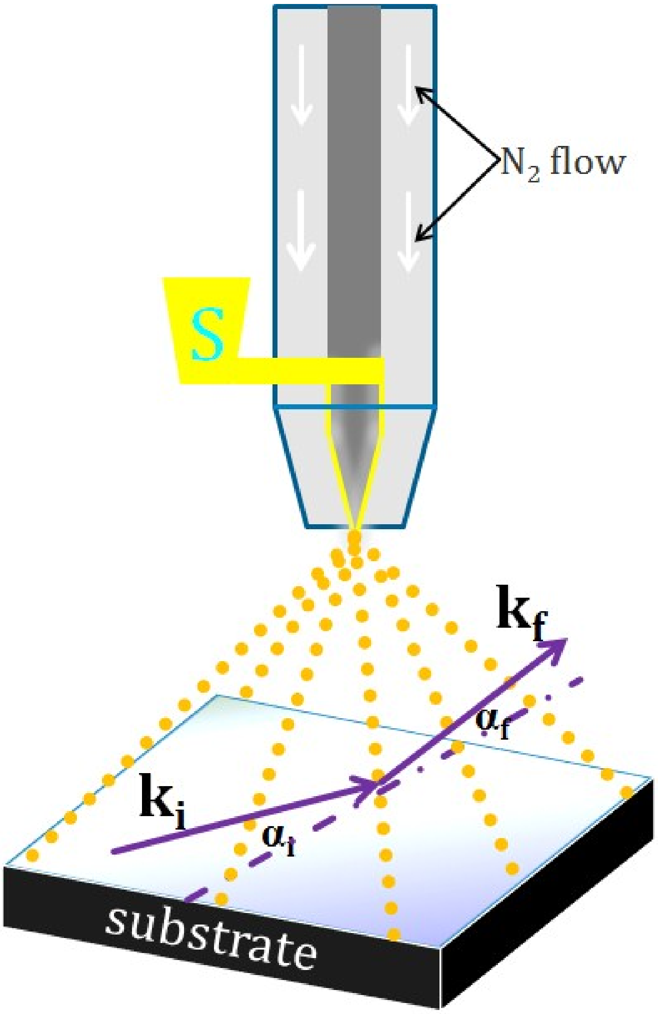

Figure S3. Illustration of *in situ* GISAXS measurement of the structure formation in air-brush spray-deposited liquid layer during solvent evaporation. k_i and k_f, α_i and α_f are the incident and scattered wave vectors, incident and exit angles, respectively. S indicates the solution tank that connected with the carrier gas (N_2 flow).

S4. Grazing Incidence Small-Angle X-ray Scattering (GISAXS)

The GISAXS measurements were performed at the microfocus endstation of the P03 beamline[5] at PETRA III of the Deutsches Elektronen Synchrotron (DESY), Germany. The X-ray wavelength and the beam size were 0.953 nm and 22 × 15 µm^2 (horizontal × vertical), respectively. A Pilatus 1M detector (Dectris Ltd., Switzerland) collected the 2D GISAXS patterns. The sample-to-detector distance was 5637 mm, calibrated by silver behenate. As shown in Figure S3, an incident wave vector k_i is scattered in the direction of k_f; α_i and α_f represent incident and exit angles, respectively. α_i was set to 0.4°, which is above the critical angles for total reflection of PEDOT:PSS, silicon substrate and Au. The corresponding X-ray illuminated area in the beam direction is ca. 2.2 mm. To reach high temporal resolution, the typical exposure time and readout times for *in situ* measurement were set at 95 ms and 5 ms, respectively. The analysis of the data was performed with the software DPDAK[6]. Note: the Yoneda peak value was taken at $\alpha_{f,\,si} + \alpha_i$ to present the structure formation during solvent evaporation.

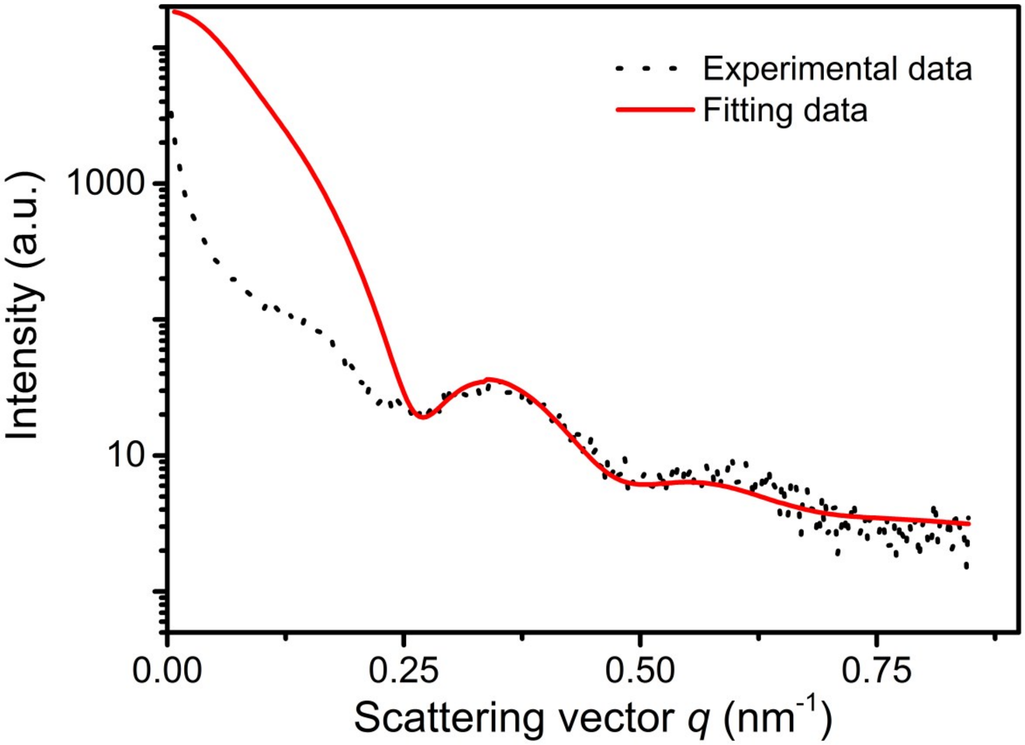

Figure S4. Horizontal integration at the silicon Yoneda peak ($\alpha_{f,\,si} + \alpha_i = 0.54°$) and the fitting with a cylinder model.

We analyzed the horizontally integrated data referring to Figure 1c by using the Scatter[3] software. Form factor for a cylinder having the radius of 14.9 ± 2 nm, and length 69.1 ± 10 nm, fits the experimental data well (Figure S4). The deviation between the fitting and experimental data at the low q values ($q < 0.25$ nm^{-1}) could be rationalized by the large scale structure of the dried AuNRs' film (for example, localized AuNR clusters as shown in SEM data of Figure 1d). The localized AuNR clusters and their scattering pattern can be fitted well with software sasfit[7] using a paracrystalline structure factor with local monodisperse approximation and assuming that the AuNRs are monodisperse, Figure S5.

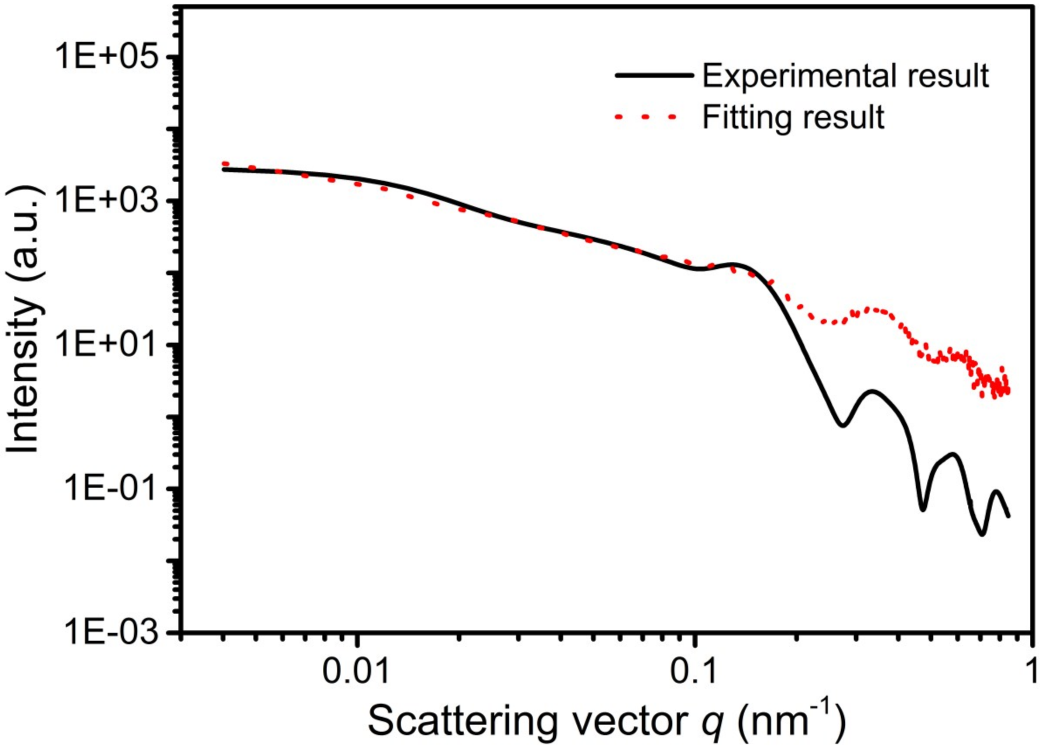

Figure S5. Horizontal integration at the silicon Yoneda peak (αf, si + αi = 0.54°) and the fit with a model using a monodisperse cylinder form factor (Radius 14.9 nm, polydispersity 0.11 and Schulz-Zimm distribution) and a paracrystalline assembly for the structure factor (mean number of stacks 4.29, stacking separation 35.8 nm, stacking disorder parameter 8.3 nm, number of uncorrelated scattering bilayer 2.9 nm and monodisperse approximation).

Fitting of the vertical integration data at q_y = 0 nm^{-1} with a cylinder model that mimics the AuNRs in Figure S1 is shown in Figure S6. The ideal cylinder form factor (with a relative standard deviation R = 0 that is different from the real system with R = 0.1) shows scattering signal that overlaps with the Yoneda peaks, e.g., Y_{Au} as marked in Figure S6, but this does not mean there is no Y_{Au}. We believe that, in the dried film as shown in Figure S6, the scattering signal around Y_{Au} consists contributions of both Y_{Au} and particle form factor. To prove this, we chose three rectangular zones that consist with (R1 in Figure S6) and without (R2, R3 in Figure S6) Y_{Au} signal and study their intensity change with solvent drying as shown in Figure S7. We find the intensity of scattering signal from particle form factor are stable in the drying stage, i.e., 1.3 s < t < 17.3 s, in Figure S7c,d. In contrast, there is a clear increase of the intensity in Figure S7b at around t = 14 s, which one can rationalize with the formation of a stable Au layer and the Au Yoneda signal increased the scattering intensity.

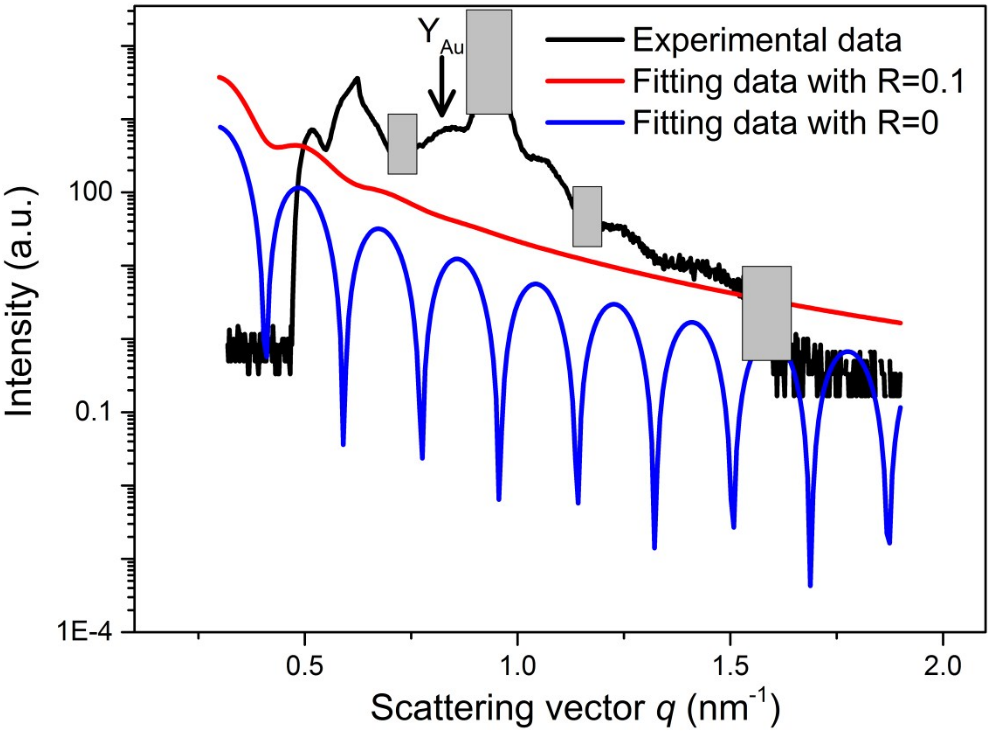

Figure S6. Vertical integration at q_y = 0 nm^{-1} and attempted fit with a cylinder model. R indicates the relative standard deviation. Grey rectangles indicate SBS and IDG.

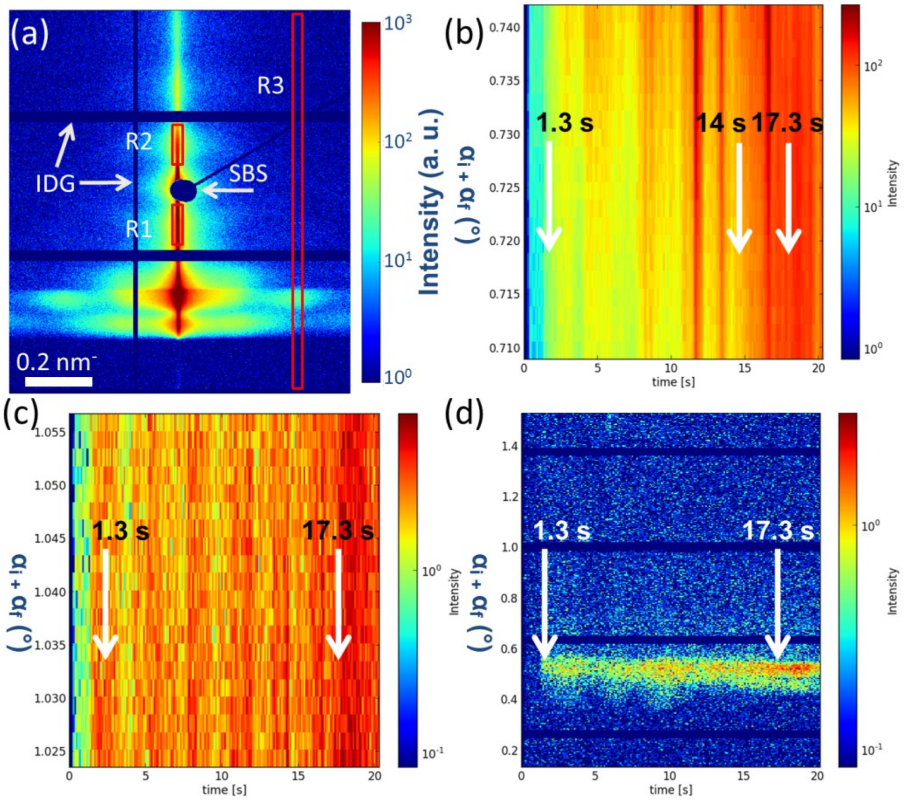

Figure S7. (a) The 2D GISAXS pattern adapted from Figure 1a show the three chosen rectangular zones consisting with (R1) and without (R2, R3) scattering signal of Y_{Au}. (b) 2D contour plot of the *in situ* GISAXS data: out-of-plane cut around Y_{Au}, marked with R1 in panel a. (c) 2D contour plot of the *in situ* GISAXS data: out-of-plane cut around $\alpha_i + \alpha_f = 1.04°$, corresponding one high order scattering of cylinder form factor in Figure S6, marked with R2 in panel a. (d) 2D contour plot of the *in situ* GISAXS data: out-of-plane cut at $q_y = 0.35$ nm^{-1}, corresponding to one high order scattering of cylinder form factor in Figure S4, marked with R3 in panel a. The time scale was set relating to the opening of the beam shutter.

S5. Evolution of tilt angle (*Φ*) with time

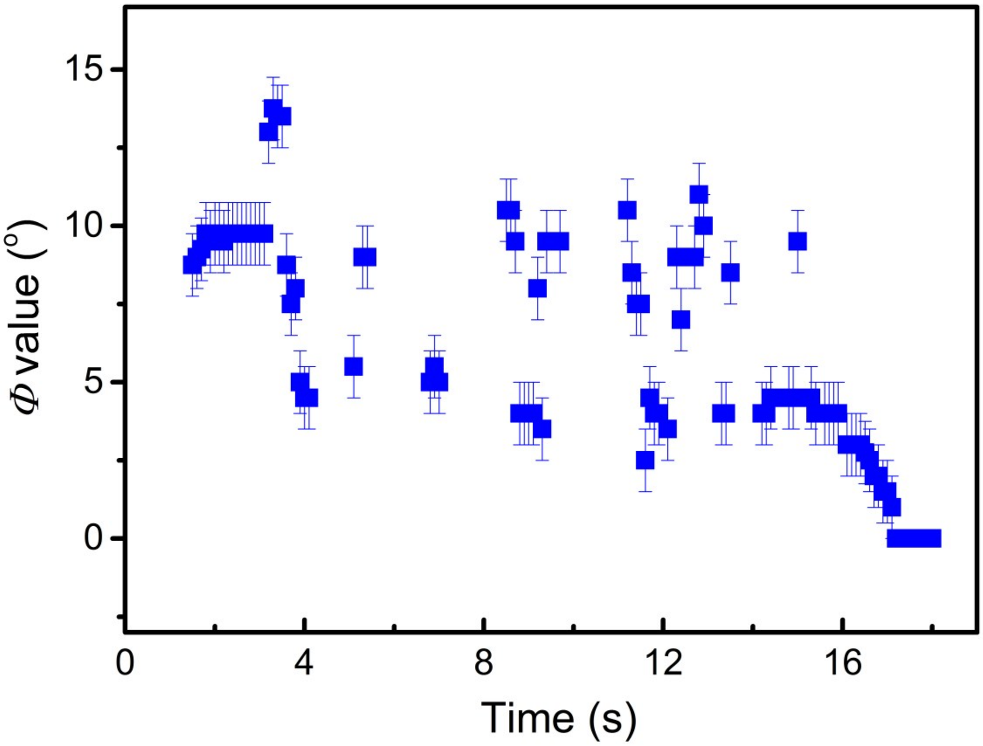

Figure S8. Change of tilt angle (*Φ*) of the prominent inclined scattering rod (indicated in Figure 2c,d) with time. The time scale was set relating to the opening of the beam shutter.

We analyze the GISAXS patterns semi-qualitatively, focusing on the prominent inclined scattering rod as marked in Figure 2c. The *Φ* is plotted as a function of time in Figure S8. The dynamic assembly of AuNRs during solvent evaporation causes the fluctuations of *Φ* values. The monotonous decrease of the angle from 4.5° to 0° in the final stage of drying corresponds to the rods stabilized on the substrate.

S6. Structure of thick spray-coated particle films

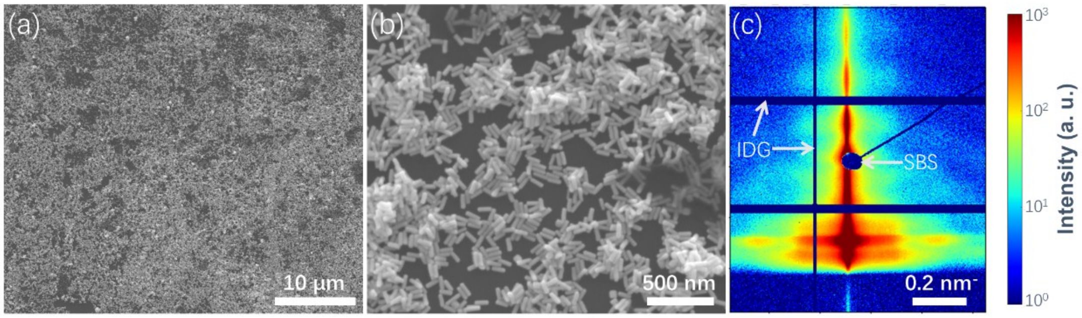

Figure S9. (a,b) Electron micrographs of a thick particle film formed by multiple spray-coating steps. (c) A typical 2D GISAXS pattern of such a film. SBS indicates the specular beam stop; the black strips labeled with IDG are due to the intermodular detector gaps.

Thick particle films were prepared by repeating the spray-coating step described previously 5 times and drying for 60 s after each step. The surface morphology of the film was characterized with scanning electron microscopy (FEI Quanta 400F, FEI Europe, Eindhoven, Netherlands, operating voltage 10 kV) as illustrated in Figure S9. GISAXS measurements of the thick film were obtained as for the monolayer.

S7. Ligand layer thickness

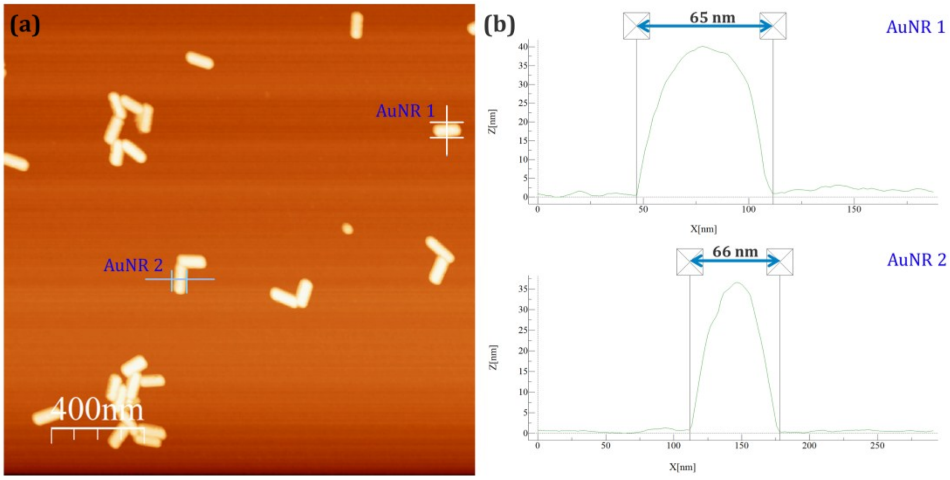

Figure S10. AFM data showing (a) the topography of the sparse monolayer and (b) height profiles of selected single AuNR particle, as marked with AuNR1 and AuNR2, respectively.

We calculated the polymer ligand layer thickness based on the AFM data (Figure S10) and SAXS data (Figure S1) that show the lateral dimensions of hybrid AuNR particle and Au core, respectively. The lateral dimension of hybrid AuNR particle (Figure S10b) is 66 nm and the radius of Au core is 17.2 ± 2 nm, and we obtain the ligand layer thickness of ca. 16 nm.

S8. Generalized two-dimensional correlation (2DC) analysis of GISAXS data

The generalized two-dimensional correlation (2DC) analysis was developed by Noda[8] to elucidate information in spectral variations of infrared, X-ray, and UV-Vis data obtained under thermal, electrical, optical or chemical perturbations.[9] Its main advantages include[10] (i) a better understanding of complex spectra with many overlapping peaks, and an enhanced effective spectral resolution by spreading peaks over the second dimension; (ii) unambiguous assignment of peaks through the correlation of bands; (iii) identification of the specific sequential order of spectral intensity changes taking place during the measurement or the value of a controlling variable affecting the spectrum through asynchronous analysis; (iv) so-called heterospectral correlation, i.e., the identification of correlation among bands in two different types of spectroscopy, for example, the correlation between IR and Raman bands.

Here, we used the 2DC analysis to analyze the Yoneda peaks' signal of GISAXS data and study the structure formation process of hybrid rod layers during solvent evaporation. The data analysis of 2DC-GISAXS was performed using the software 2DShige by Shigeaki Morita, Kwansei-Gakuin University, 2004-2005. We briefly describe the basic concept of 2DC-GISAXS in the following, referring to the principles of generalized 2DC spectroscopy[9].

In 2DC-GISAXS, vertically integrated GISAXS data A (α_j, t_i) is obtained as a function of the scattering angles α_j with j=1, 2, ⋯⋯n and time variables t_i with i=1, 2, ⋯⋯m during the observation interval between t_1 and t_m. The liquid evaporation induced dynamic GISAXS spectra were transformed into a set of 2DC-GISAXS spectra by a cross correlation analysis. We describe the principles of cross correlation analysis in the following.

The dynamic GISAXS data Ã (α_j, t_i) from the evaporating film was defined within the observation intervals between t_1 and t_m as

$$\tilde{A}\ (\alpha_j,\ t_i) = A\ (\alpha_j,\ t_i) - \bar{A}\ (\alpha_j,\ t_i)$$

Where Ā (α_j, t_i) is the reference spectrum of the system; here we selected the averaged spectrum which is given by

$$\bar{A}\ (\alpha j,\ ti) = \frac{1}{m}\sum_{i=1}^{m} A\ (\alpha_j,\ t_i)$$

Synchronous (Φ) and asynchronous (Ψ) correlations spectra are given by

$$\Phi(\alpha_{x,}\ \alpha_y) = \frac{1}{m-1}\sum_{i=1}^{m}\tilde{A}\ (\alpha_x,\ t_i)\cdot\tilde{A}\ (\alpha_y,\ t_i)$$

$$\Psi(\alpha_x,\ \alpha_y) = \frac{1}{m-1}\sum_{i=1}^{m}\tilde{A}\ (\alpha_x,\ t_i)\cdot\sum_{k=1}^{m}N_{ik}\tilde{A}\ (\alpha_y,\ t_k)$$

Where N_{ik} is the Hilbert-Noda transformation matrix given by

$$N_{ik} = \begin{cases} 0 & if\ i = k \\ \dfrac{1}{\pi \cdot (k - i)} & otherwise \end{cases}$$

We interpreted the 2DC-GISAXS data and determined the sequence of structure formation during liquid evaporation by following Noda's rules[10]:

1. If the intensities of α_x and α_y in the *GISAXS* dataset are changing in the same direction, the synchronous 2D cross peak at (α_x, α_y) is positive;

2. if the intensities of α_x and α_y in the *GISAXS* dataset are changing in the opposite direction, the synchronous 2D cross peak at (α_x, α_y) is negative;

3. if the change at α_x mainly precedes the change at α_y, the asynchronous 2D cross peak at (α_x, α_y) is positive;

4. if the change at α_x mainly follows the change at α_y, the asynchronous 2D cross peak at (α_x, α_y) is negative;

5. if the synchronous 2D cross peak at (α_x, α_y) is negative, the interpretation of rule 3 and 4 for the asynchronous 2D peak at (α_x, α_y) has to be reversed.

S9. Porous structure of a polystyrene reference monolayer

To prove the existence of a porous structure in the hybrid rod layer, polystyrene nanoparticles (PPs-0.1) with nominal diameter of 100 nm (measured with dynamic light scattering) from Kisker Biotech GmbH & Co. KG, Germany were used as a model. We performed a series of experiments to show that the GISAXS peak at $\alpha_i + \alpha_f = 0.49°$ (Figure S11 and S12), corresponding to the porous structure in PS colloidal layer (Figure S13a), shifts to high exit angles at high thermal-annealing temperatures due to melting and merging of the colloidal structure at $T > T_g$ (glass transition temperature of bulk PS, ca. 100 °C). Densely packed PS domains were observed at T=120 °C (Figure S13b).

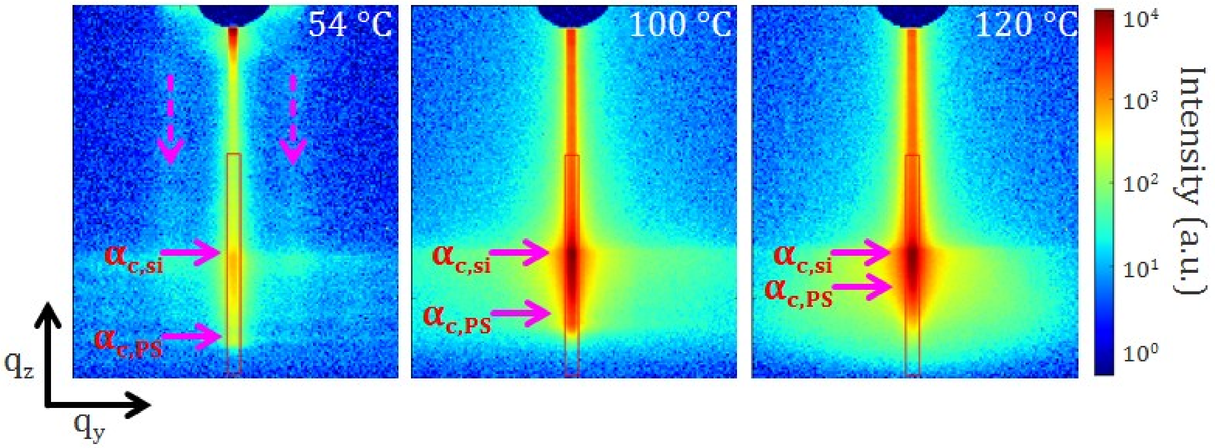

Figure S11. Typical 2D GISAXS patterns of a PS colloidal layer thermally annealed at different temperatures, i.e., 54 °C, 100 °C and 120 °C. The Yoneda peak positions of porous structure of the PS monolayer ($\alpha_i + \alpha_{c,PS}$) and the silicon substrate ($\alpha_i + \alpha_{c,Si}$) are marked with solid arrows. Two side streaks symmetrically distributed regarding the scattering plane (q_y = -0.069 and 0.069 nm^{-1}) were observed (marked with dashed arrows) only in the sample prepared at 54 °C. These streak signals corresponded to the nanoparticle diameter of 91 nm, indicating a close packing of the adjacent nanoparticles[4, 11]; the disappearing of these streaks in samples that were annealed at 100 °C and 120 °C indicate that the ordered structure were destroyed due to merging of the nanoparticles at $T > T_g$.

The PS nanoparticles were well dispersed in water with concentration 2.5 wt%. A dispersion for air-brush spray application was diluted with an equal volume of ethanol to accelerate solvent evaporation. A PS colloidal porous layer on silicon substrate (Figure S13) was sprayed in 0.1 s at an argon carrier gas pressure of 1 bar as demonstrated in the previous work.[4]

GISAXS measurements were undertaken at the P03 beamline of DESY using an X-ray wavelength of 0.1088 nm, a beam size of 28 × 24 μm^2 (horizontal × vertical), sample-to-detector distance 4057 mm, exposure time 95 ms, and $\alpha_i = 0.45°$. A hot stage (DHS 1100, Anton Paar GmbH, Austria) was used to control the substrate temperature at set values.

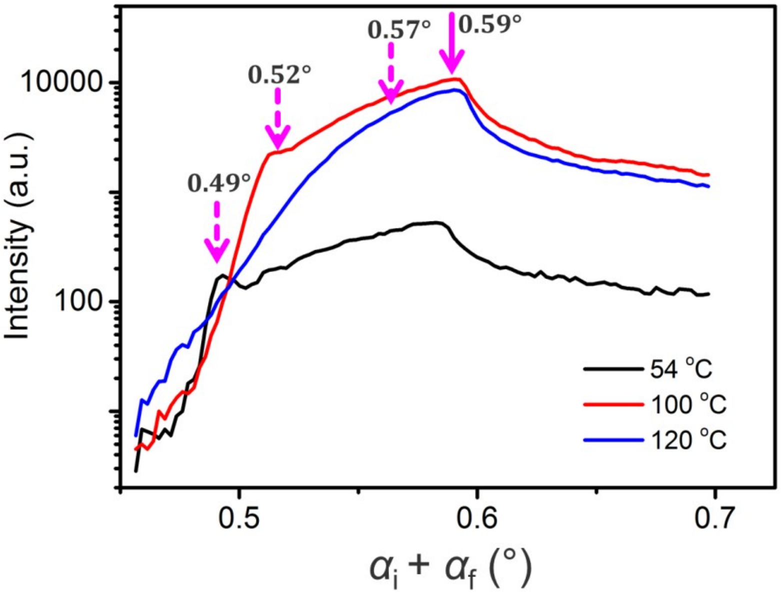

Figure S12. Vertical integration along the rectangular zones marked in Figure S11. The Yoneda peak positions of the porous structure in PS colloidal layer at different substrate temperatures were marked with dashed-arrows in the curves; the Yoneda peak position of silicon substrate was marked with solid arrow.

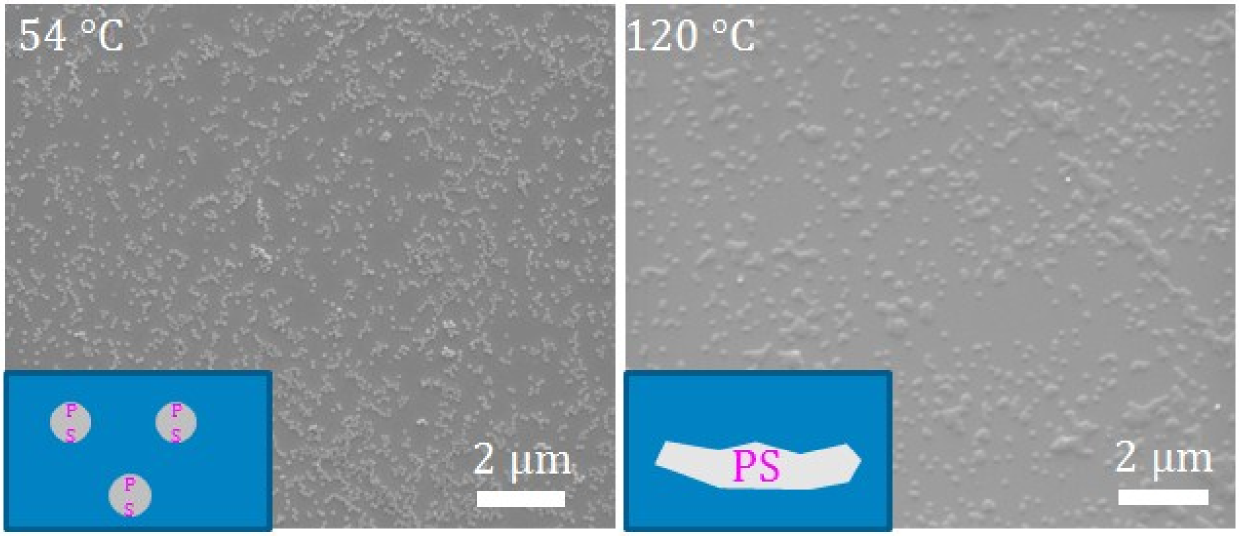

Figure S13. Scanning electron microscopy data showing surface morphologies of the spray-deposited PS nanoparticles thermally annealed at substrate temperatures of (a) 54 °C and (b) 120 °C. Inserted cartons indicate the nanoparticles changed from well-shaped PS nanospheres (a) to densely packed PS domains (b) due to melting of PS and merging of the nanoparticles.

S10. Zeta potential measurements

Zeta potentials were measured with a Litesizer^{TM} 500 setup (Anton Paar, Graz, Austria). 1 mM $NaNO_3$ aqueous solution was used for the sample preparation and the sample was held in an omega-shaped zeta potential cuvette. We did the measurements at 25 °C and data analysis with the Smoluchowski model.

For PEDOT:PSS dispersion, the mean zeta potential was 0.2 mV with a standard deviation of 0.7 mV; for Au-PEDOT:PSS hybrid nanoparticle dispersion, the mean zeta potential was -24.9 mV with standard deviation of 1.0 mV.

References:

(1) Ye, X.; Zheng, C.; Chen, J.; Gao, Y.; Murray, C. B. Using Binary Surfactant Mixtures To Simultaneously Improve the Dimensional Tunability and Monodispersity in the Seeded Growth of Gold Nanorods. *Nano Lett.* **2013,** *13* (2), 765-771, DOI: 10.1021/nl304478h.

(2) Reiser, B.; Gonzalez-Garcia, L.; Kanelidis, I.; Maurer, J. H. M.; Kraus, T. Gold nanorods with conjugated polymer ligands: sintering-free conductive inks for printed electronics. *Chem. Sci.* **2016,** *7* (7), 4190-4196, DOI: 10.1039/c6sc00142d.

(3) Forster, S.; Apostol, L.; Bras, W. Scatter: software for the analysis of nano- and mesoscale small-angle scattering. *J Appl Crystallogr* **2010,** *43* (3), 639-646, DOI: doi:10.1107/S0021889810008289.

(4) Zhang, P.; Santoro, G.; Yu, S.; Vayalil, S. K.; Bommel, S.; Roth, S. V. Manipulating the Assembly of Spray-Deposited Nanocolloids: In Situ Study and Monolayer Film Preparation. *Langmuir* **2016,** *32* (17), 4251-4258, DOI: 10.1021/acs.langmuir.6b00892.

(5) Buffet, A.; Rothkirch, A.; Döhrmann, R.; Körstgens, V.; Kashem, M. M. A.; Perlich, J.; Herzog, G.; Schwartzkopf, M.; Gehrke, R.; Müller-Buschbaum, P.; Roth, S. V. P03, the microfocus and nanofocus X-ray scattering (MiNaXS) beamline of the PETRA III storage ring: the microfocus endstation. *J. Synchrotron. Radiat.* **2012,** *19*, 647-653, DOI: Doi 10.1107/S0909049512016895.

(6) Benecke, G.; Wagermaier, W.; Li, C. H.; Schwartzkopf, M.; Flucke, G.; Hoerth, R.; Zizak, I.; Burghammer, M.; Metwalli, E.; Muller-Buschbaum, P.; Trebbin, M.; Forster, S.; Paris, O.; Roth, S. V.; Fratzl, P. A customizable software for fast reduction and analysis of large X-ray scattering data sets: applications of the new DPDAK package to small-angle X-ray scattering and grazing-incidence small-angle X-ray scattering. *J Appl Crystallogr* **2014,** *47*, 1797-1803, DOI: 10.1107/S1600576714019773.

(7) Bressler, I.; Kohlbrecher, J.; Thunemann, A. F. SASfit: a tool for small-angle scattering data analysis using a library of analytical expressions. *J Appl Crystallogr* **2015,** *48*, 1587-1598, DOI: 10.1107/S1600576715016544.

(8) Noda, I. Two-dimensional infrared spectroscopy. *Journal of the American Chemical Society* **1989,** *111* (21), 8116-8118, DOI: 10.1021/ja00203a008.

(9) Park, Y.; Noda, I.; Jung, Y. M. Two-dimensional correlation spectroscopy in polymer study. *Frontiers in Chemistry* **2015,** *3* (14), DOI: 10.3389/fchem.2015.00014.

(10) Noda, I.; Ozaki, Y. *Two-Dimensional Correlation Spectroscopy—Applications in Vibrational and Optical Spectroscopy*, John Wiley & Sons, Ltd: New York, 2004.

(11) Herzog, G.; Benecke, G.; Buffet, A.; Heidmann, B.; Perlich, J.; Risch, J. F. H.; Santoro, G.; Schwartzkopf, M.; Yu, S.; Wurth, W.; Roth, S. V. In Situ Grazing Incidence Small-Angle X-ray Scattering Investigation of Polystyrene Nanoparticle Spray Deposition onto Silicon. *Langmuir* **2013,** *29* (36), 11260-11266, DOI: 10.1021/la402254q.